Journal of Colloid and Interface Science 598 (2021) 155–165

Contents lists available at ScienceDirect

Journal of Colloid and Interface Science

journal homepage: www.elsevier.com/locate/jcis

Regular Article

A carbon ink for use in thin, conductive, non peelable, amphiphilic, antioxidant, and large-area current collector coating with enhanced lithium ion battery performance

Kuan-Ting Chen, Yi-Chun Yang, Yuan-Hsing Yi, Xiang-Ting Zheng, Hsing-Yu Tuan *

Department of Chemical Engineering, National Tsing Hua University, Hsinchu 30013, Taiwan

GRAPHICAL ABSTRACT

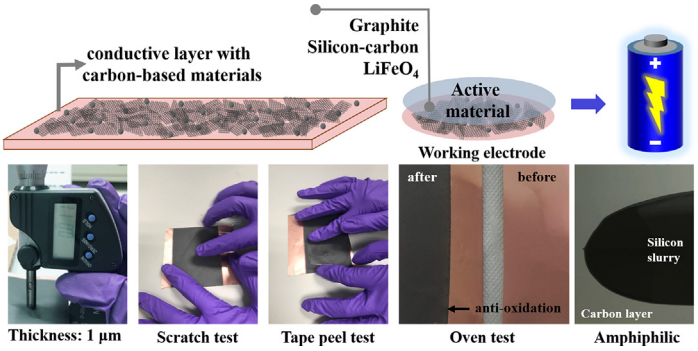

ARTICLE INFO

Article history:
Received 11 February 2021
Revised 24 March 2021
Accepted 25 March 2021
Available online 29 March 2021

Keywords:
Conductive layer
Ball milling
Current collector
Carbon coated copper foil
Lithium ion battery
Anode materials

ABSTRACT

We reported that a stable carbon ink composed of conductive carbon materials (graphene and super P), binder (sodium carboxymethyl cellulose (CMC)), interface active agent (sodium dodecyl sulfate (SDS)), and metal coupling agent ((3-aminopropyl)triethoxysilane (APTES)) for using in coating conducting layer on cathode/anode current collector for LIBs. Graphene materials are obtained using a low-cost graphite material (KS 6) and processing it via a wet ball-milling to exfoliate single layers into the ink. The ink can be coated on the LIB current collector in a large area by a doctor blade to form a carbon layer of about 1 μm without overflow. Carbon-coated current collectors have amphiphilic properties, not peel off under extreme physical and chemical conditions, and resist oxidation under high temperature (200 °C) processing conditions. In addition, carbon-coated current collector are superior to the batteries using bare metal foil a current collectors in the LIB performance of graphite half-cell, graphite full-cell, $LiFePO_4$ half-cell, and silicon-carbon full-cell. These results show that the carbon-coated metal foil can reduce the interface resistance with the active material and improves the adhesion of the active materials to the current collector, avoiding peeling off during charge/discharge process, thereby improving of LIBs performance. The developed method can produce high-quality, low-cost carbon material inks on a large scale through a simple and inexpensive process, and coat them evenly and finely on current collectors, making it possible to achieve efficient industrial and commercial perspectives for next-generation LIB-based current collectors.

* Corresponding author.
E-mail address: hytuan@che.nthu.edu (H.-Y. Tuan).

https://doi.org/10.1016/j.jcis.2021.03.146
0021-9797/

1. Introduction

LIB electrodes are commonly prepared in the form of slurries composed of the active materials, conductive additives and polymer adhesives and then coated on a current collector. The current collector, *i.e.*, copper foil or aluminum foil, collects and transmits electrons through physical contact between the active material and the current collector [1]. By enhancing the adhesion and reducing the resistance of the interface, the cycle stability of the battery can be greatly improved. When a lithium ion battery is operating, the volumes of active material will expand and contract due to insertion and extraction of lithium ions, which will cause the electrode materials to peel off from the current collector and fast capacity decay. For example, the volume change of active material (graphite) during the lithiation/delithiation process is about 13% [2,3]; however, continuous volume changes can form an unstable solid electrolyte interphase (SEI), and the capacity and electrochemical performance are poor due to associated strain caused by the large contact resistance. High-capacity commercially ready electrode materials, silicon-carbon anodes, are more affected by dramatic changes in volume because the volume change of silicon changes up to ~ 400% during cycling [4–8]. During repeated lithiation/delithiation cycles, most commercially available binders cannot endure the strain caused by volume change of silicon.

Surface treatment of the copper foil can improve the adhesion between the material and the current collector, reduce the internal resistance of the LIB, and extend battery life. There are currently two methods of collector surface treatment. One is to form an uneven rough surface by chemically etching the current collector [9,10], but this method requires high processing requirements, is expensive, and is not suitable for mass production. The other is to coat a thin layer of conductive material on the surface of the current collector [11–13]. The material needs to have good conductivity, high specific surface area, good adhesion, and better deformability relative to the metal current collector so as to reduce the interface resistance and improve bonding strength. This method is relatively simple in operation and low in cost, and is the main development direction for surface modification of current collector.

Carbon-based materials are the most widely used conductive layer materials because of their low cost, no oxidation and easy handling. However, powder agglomeration and uneven dispersion often occur because powdered materials have high specific surface area and high surface energy in the process of coating carbon slurry on the current collector surface. In order to reduce the surface energy, most powdered materials have different degrees of aggregation through some paths and mechanisms, including electric charge, osmotic pressure, Van der Waals force, bridging surface *etc.*, resulting in hard and soft agglomeration of the powder. Common solutions can be summarized in two categories: one is mechanical grinding; the other is chemical method. In mechanical methods, wet milling is mainly used to solve hard agglomerations combined with high-power ultrasonic dispersion to improve soft agglomeration [14–16]. On the other hand, the main challenging of chemical methods is to prevent reaggregation [17]. The coupling agent is often added into carbon-based ink to simultaneously bond with the inorganic functional groups on the surface of the carbon materials and the current collector, and significantly improving the bonding strength of the interface [18]. In an acidic aqueous solution, the functionalized graphene was coated on the steel plate, and after a tape peel test, it was found that the coating has good adhesion without peeling. Due to the limited dispersion stability of graphene flakes, a large amount of solvent is always required in certain purification and dispersion methods. Graphene can only be dispersed in a small amount (<1 mg mL^{-1}) in common solvents [19–21], yet the dispersibility can be improved by dispersing agents or prolonged ultrasonic treatment. Reducing the amount of solvent make the graphene dispersion unstable, and only a small amount of graphene is produced. Additionally, the thickness of the carbon conductive layer is also critical because a thicker coating reduce the volume capacity of the battery. When the electrode in in contact with the liquid electrolyte in the potential window of the electrode, the carbon-coated current collector has high conductivity to reduce battery resistance and improve chemical stability.

Therefore, the contact surface between current collector of lithium-ion batteries (LIBs) and the active material requires an effective buffer layer to reduce the interface resistance and improve the stability and performance of batteries. However, the existing main methods, such as chemical etching or thin layer coating of conductive material on the surface of the current collector, have limitations in terms of high cost, low quality, poor productivity, environmental issues, and failed to prove its sufficient commercialization potential to meet the market's demand for multiple purposes. In this study, we report a carbon ink coating on the surface of current collector to form a 1 μm thin coating layer which has good conductivity, high specific surface area, oxidation resistance, and strong bonding with the current collector. As shown in Scheme 1, the ink components include conductive carbon materials (graphene and super P), binder (sodium carboxymethyl cellulose (CMC)), interface active agent (sodium dodecyl sulfate (SDS)), and metal coupling agent ((3-Aminopropyl)triethoxysilane (APTES)). The ink can be coated on a large area by a doctor blade or other coating process to form a carbon layer of about 1 μm. The carbon conductive layer has many excellent properties, including an amphiphilic surface, no peeling off under extreme physical and chemical conditions, and high-temperature anti-oxidation. The effects of carbon coated metal foil on graphite half-cell, graphite full-cell, $LiFePO_4$ half-cell, and silicon-carbon full-cell on LIBs were investigated, showing the cycle life, adhesion of the active materials and current collector, and rate capability using carbon-coated current collectors are all better than bare metal foil.

2. Materials and methods

2.1. Materials

Sodium carboxymethyl cellulose (CMC), sodium dodecyl sulfate (SDS) and 1-methyl-2-pyrrolidinone (NMP, anhydrous, 99.5%) were purchased from Sigma-Aldrich. KS6, lithium hexafluorophosphate ($LiPF_6$), fluoroethylene carbonate (FEC, $C_3H_3FO_3$), diethyl carbonate (DEC, $C_5H_{10}O_3$), ethylene carbonate (EC, $C_3H_4O_3$), membrane, super-P, Poly(vinylene fluoride), and coin-type cell CR2032 were purchased from Shining Energy Co. Ltd. (3-Aminopropyl)triethoxysilane (APTES) was purchased from Alfa Aesar. Poly (acrylic acid) (PAA, average Mv ~ 3000000) was purchase from Aldrich. Glass fibers (diameter = 19 mm) were purchased from Advantec. Commercial $LiFePO_4$ cathode materials were purchased from Vista Advance Technology. The components of pouch type battery were purchased from MTI Shenzhen kejingtar technology. LEDs were purchased from an electronic equipment and appliance store. The tape was purchased from Symbio, inc.

2.2. Preparation of carbon ink

First, 3 g KS6, 1.25 g CMC, 0.75 g super p, 0.5 g SDS and DI water were mixed uniformly and sealed into ball-milling jar. Then, the carbon ink was obtained by wet ball milling for 2 h. Before coating on copper foil, APTES was added to the carbon ink.

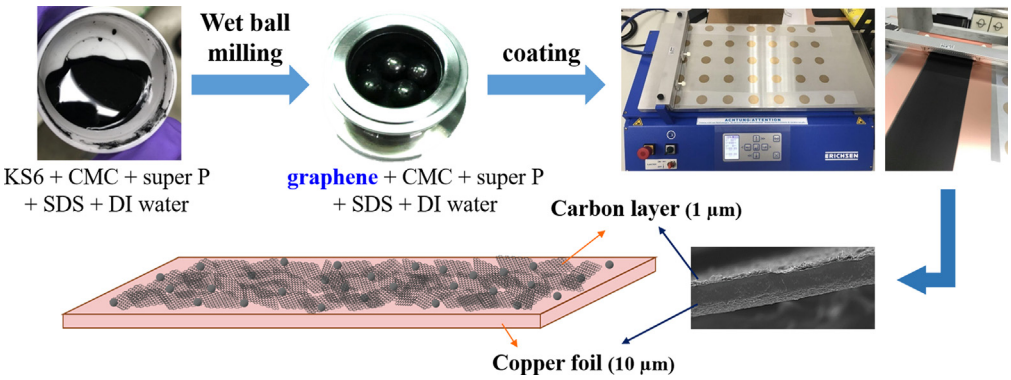

Scheme 1. Schematic diagram showing formation of the carbon-coated copper foil.

2.3. Material characterizations

The morphologies and the microstructure of the prepared samples were investigated using scanning electron microscopy (HITACHI-SU8010) with energy-dispersive X-ray spectroscopy (HORIBA, EX-250) and spherical aberration corrected scanning transmission electron microscope (JEOL, ARM200F). The adhesion between materials and current collectors was investigated by universal testing machine (Instron 3343). The electrochemistry impedance spectroscopy test and the cyclic voltammetry test were measured by using VMP3 (Bio-Logic Science Instruments).

2.4. Electrochemical measurements

Graphite was mixed with Super P and PVDF binder in a weight ratio of 8:1:1 and dispersed in NMP to prepare the slurry coating on the bare copper foil and carbon-coated copper foil for graphite half-cell and full-cell. The average mass loading of active material (graphite) is ~5.9 mg cm^{-2}. To prepare a NCM cathode, the NCM was mixed with Super P and CMC in a weight ratio of 90:5:5, which was spread on an aluminum foil for graphite coin-type full cell. For a pouch-type full cell, graphite anode and commercial NCM cathode electrodes were cut into the area of 9 cm^2. $LiFePO_4$ was mixed with Super P and PVDF binder in a weight ratio of 90:5:5 and dispersed in NMP to prepare the slurry coating on the bare aluminum foil and carbon-coated aluminum foil for positive half-cell. The average mass loading of active material ($LiFePO_4$) is ~13 mg cm^{-2}. Silicon power and graphite (silicon power : graphite = 20:80) were mixed with Super P and PAA binder in a weight ratio of 76:9:15 and dispersed in ethanol to prepare the slurry coating on the bare copper foil and carbon-coated copper foil for silicon-carbon half-call and full-cell. The average mass loading of active material (silicon-carbon) is ~4.6 mg cm^{-2}. To prepare a NCM cathode, the commercial NCM was uesd for silicon-carbon full-cell. The electrochemical properties of the as-prepared electrodes were evaluated by assembling CR 2032-type coin cells in the argon filled glovebox. For graphite half-cell and full cell, 1 M $LiPF_6$ (in EC:DEC = 1:1) as the electrolyte. For positive half-cell, 1 M $LiPF_6$ (in EC:DEC = 1:2) as the electrolyte.

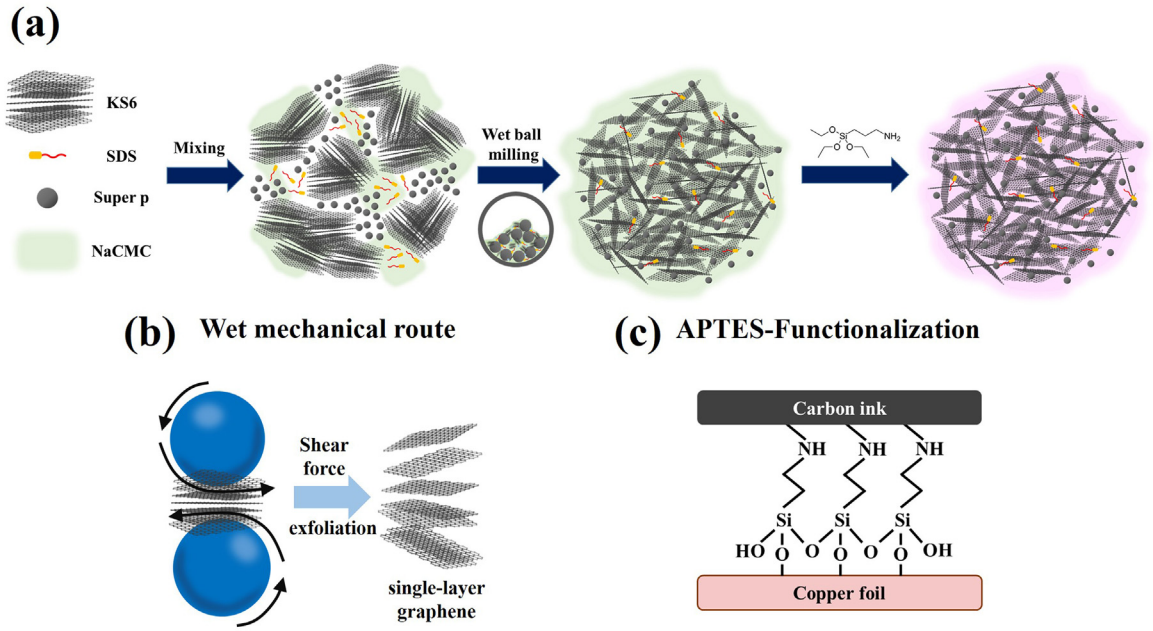

Fig. 1. Principle of preparation of carbon ink: (a) KS6, CMC, super p, SDS and DI water were mixed and sealed into ball-milling jar. Then, the homogeneous carbon ink was obtained by wet ball milling where graphene layers were produced during milling. Before coating on copper foil, APTES was added to the carbon ink. (b) Single layers of graphene were exfoliated from KS6 via shear force. (c) The amino group of APTES can form a chemical bond to the carbon materials and the metal substrate and establish a chemical network to increase adhesion.

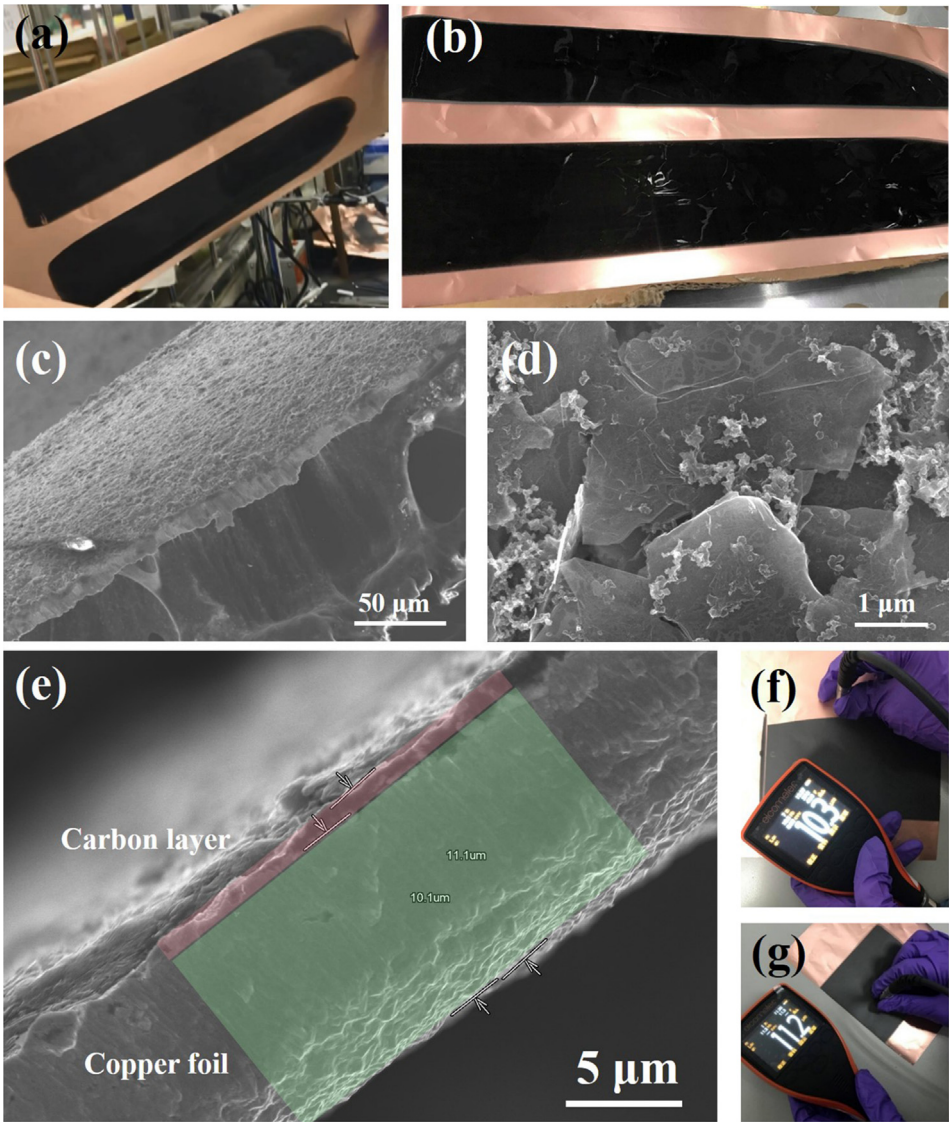

Fig. 2. Characterization of carbon-coated copper foil. (a) The copper foil was directly picked up vertically after coating and (b) stood vertically for 1 min. SEM images of (c, e) cross-section and (d) front surface of carbon-coated layer. (f, g) The thickness of carbon-coated copper foil was measured by the thickness gauge.

For silicon-carbon half-cell and full-cell, 1 M $LiPF_6$ (in FEC:DEC = 3:7) as the electrolyte. The electrochemical performance data was collected using a Maccor Series 4000 battery test system at the voltage of 0.01–1.5 V electrode for graphite half-cell and silicon-carbon half-cell, 2.5–4.2 V for graphite coin-type and pouch-type full-cell and 2.5–4 V electrode for positive half-cell.

3. Results and discussion

Liquid phase exfoliation is a promising method to achieve scalable production of high-quality graphene or other layered materials. The use of mechanical cracking method is a green synthesis method that does not require the aid of other chemicals to make the obtained graphene impure. Fig. 1 shows the principle of mixing KS6, CMC, super P, SDS and water uniformly to form a graphene composite slurry by wet ball milling. In this method, mechanical shear force can overcome the attraction force between the KS graphite layers, so that large pieces of graphite can be peeled layer by layer to form graphene flakes [21–24]. Ideally, the graphene sheet can be peeled from the bulk graphite layer by layer, and the resistance of the van der Waals attraction between adjacent graphene sheets can be overcome. How to balance the attractiveness and the peeling layer is critical. Wet ball milling is used instead of dry ball milling, because dry ball milling usually grinds graphite into small pieces by impact or compression during the rolling process, sometimes even destroying the crystal structure of materials to form an amorphous phase [25]. Wet ball milling can produce high-quality and large-size graphene [26], and in addition, high speed impact between ball-milling tank and the steel ball generate enough kinetic energy for the bond breaking in the aromatic graphite structure where the C—C bonds are broken to create a new surface [26–28]. During grinding process, the reaction zone on the graphene surface can be controlled via tuning ball-milling conditions and introducing functional groups on the edges and surfaces of graphene-based materials. Carbon black has high slurry stabilization ability, high chemical inertness and low cost, so we add it to the slurry for carbon slurry stabilization [29–31], Carbon black can stabilize the slurry to prevent segregation, *e.g.*, sedimentation or agglomeration, and therefore support the formation of a homogeneous electrode. It is beneficial to promote the graphene sheet system through the development of the gel network, which form homogeneous conductive pathways for electron transport.

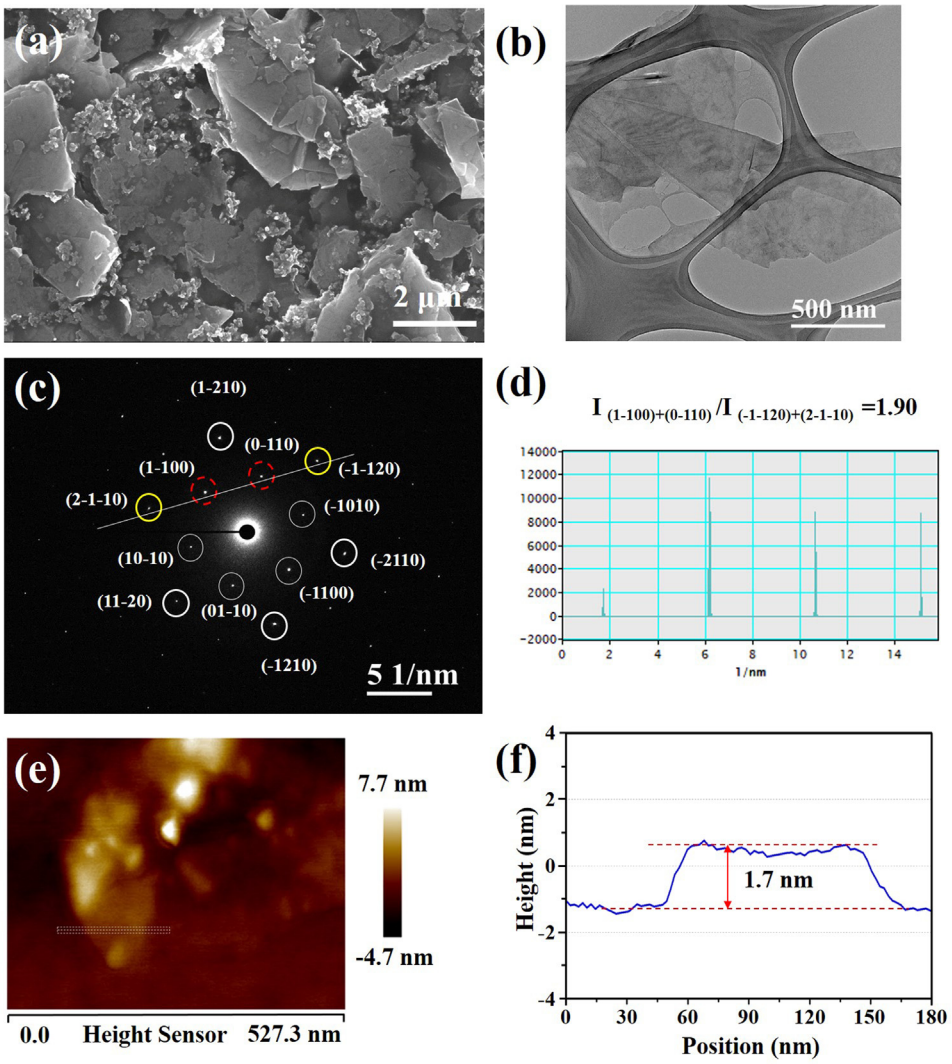

Fig. 3. Materials fabrication and structural characterization of carbon ink. (a) SEM, (b) TEM and (c) SAED images of carbon-coated layer. (d) Intensity profile through the diffraction spots labeled in figure c. (the yellow solid circle and the red dotted circle). (e) AFM images of carbon-coated layer. (f) Height profile of corresponding carbon-coated layer along the lines indicated in figure e. (For interpretation of the references to colour in this figure legend, the reader is referred to the web version of this article.)

After the carbon black is added, it can be distributed next to the graphene sheets so as to create a continuous conductive path from the current collector to each particle of the conductive carbon layer with the smallest addition amount. Since the particle size of many active materials is in the range of several microns, it is also beneficial to provide additional contact points and cover the particle surface with other conductive paths. The ratio of KS6 to carbon black was tuned to adjust the strength of the attractive force to withstand gravity that prevent the electrode coating process from complete fluidize. As shown in Fig. 2a, the carbon-coated copper foil was directly picked up vertically after coating and stood vertically for 1 min (Fig. 2b). The addition of the surfactant (SDS) enhances the diffusion of hydroxide ions, prevents the super P and graphene layer agglomeration, and increases the contact angle of water on hydrophobic graphene [32]. Finally, the coupling agent APTES is added to the prepared carbon ink, where the amino group of APTES can form a chemical bond to the carbon materials and the metal substrate and establish a chemical network to increase adhesion [18,33–35]."

As shown in Fig. 2, the carbon ink is coated on a copper foil via a blade coating to form a conductive carbon coating. The viscosity of carbon ink measured by a digital display rotary viscometer is around 7.51 cp (Table S1). When the carbon-coated copper was picked up vertically after coating (Fig. 2a) or left standing for 1 min (Fig. 2b), it was found that there was no overflow situation. The scanning electron microscopy (SEM) images of the surface topography of the carbon-coated copper foil show a uniform and dense carbon layer without bare copper (Fig. 2c and d). Under high magnification, the carbon materials are sheet-like and tightly attached to the copper foil. As shown in Fig. 2e-g, by SEM, the thickness of the carbon–coated is about 1 μm. The thickness of the carbon-coated copper foil was also measured by a thickness gauge (Fig. 2f and g), indicating that the thickness of carbon-coated copper foil is 11 μm. Therefore, the thickness of carbon-coated layer is about 1 μm after subtracting the 10 μm bare copper foil.

The SEM and transmission electron microscope (TEM) images of the carbon material were acquired, as shown in Fig. 3a and b. Fig. 3c and d show the selected area electron diffraction (SAED) patterns of carbon material to confirm their crystallinity. The relative intensity of $[1\bar{1}00]$ and $[2\bar{1}\bar{1}0]$ reflections can be used to distinguish single-layer graphene from multilayer graphite [36–38]. Fig. 3d shows that the internal $1\bar{1}00$-type reflection is stronger

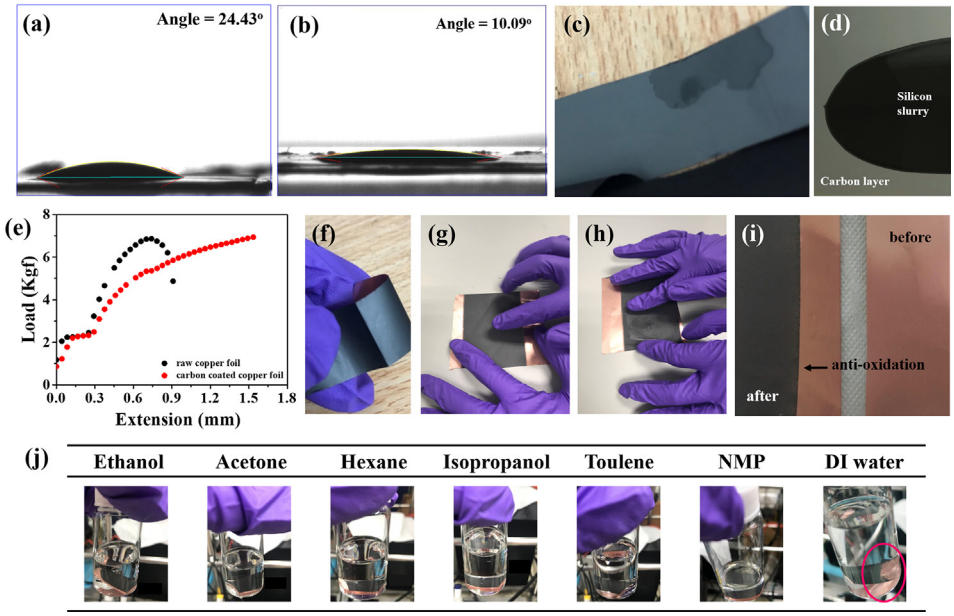

Fig. 4. Characterization of the carbon-coated copper foil. Contact angles of (a) water and (b) NMP on carbon-coated copper foil. The appearance of (c) water droplets and (d) silicon slurry on carbon-coated copper foil. (e) Tensile test of bare copper foil and carbon coated copper foil. (f) 90° bending of carbon-coated copper foil. (g) Scratch test (movie S1 showing scratch test of carbon-coated copper foil), (h) tape peel test (movie S2 showing tape peel test of carbon-coated copper foil) and (i) anti-oxidation test of carbon-coated copper foil. (j) Solvent resistance of carbon-coated copper foil in different solvents. (polar solvents: ethanol, isopropanol, NMP, and DI water; non-polar: acetone, hexane, and toluene).

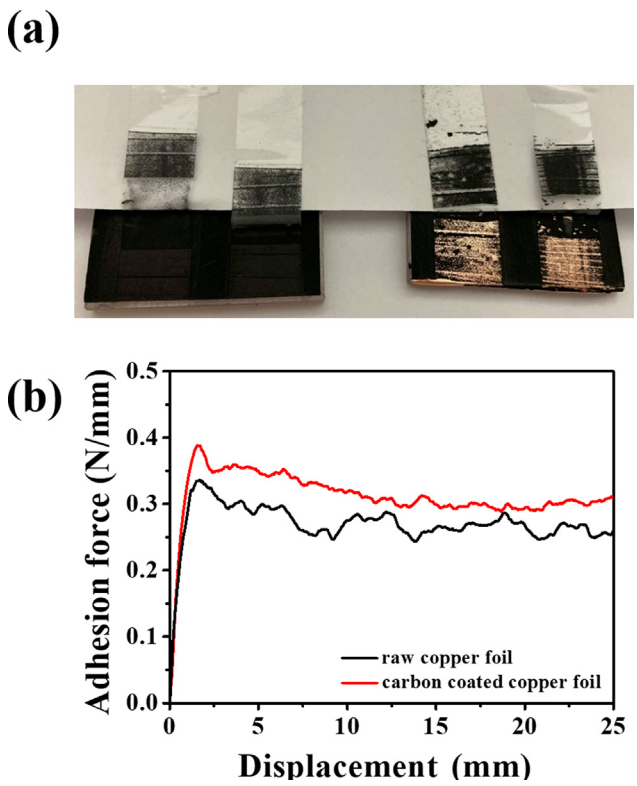

Fig. 5. (a) Adhesion test of carbon-coated layer on bare copper foil (right) and carbon-coated copper foil (left) with active material slurry by tape peel test. (b) Adhesion force for carbon-coated layer on bare copper foil and carbon-coated copper foil with slurry.

than the external $2\bar{1}\bar{1}0$-type reflection, and its ratio is around 1.9, indicating that the carbon material is a single layer instead of multilayer. Moreover, the thickness of the carbon material was revealed around 1.7 nm by Atomic force microscopy (AFM) (Fig. 3e and f).

Table 1
Volume conductivity of bare copper foil and carbon-coated copper foil.

	bare copper foil	carbon-coated copper foil
Volume conductivity (Ω•cm)	$6.79*10^{-7}$	$4.64*10^{-7}$

Fig. 4a shows that the surface of the carbon-coated copper foil is hydrophilic (10 ~ 90°) with a contact angle of 24.4°, whereas the contact angle of commercial carbon-coated copper foil (Figure S1) is hydrophobic (90 ~ 120°) with a contact angle of 129.68°. In addition, the contact angle of a common slurry solvent, NMP, is only 10.09° (Fig. 4b). The contact angle measurements show that the surface of the carbon-coated copper foil is amphiphilic. Actually, water dripping on the carbon-coated copper foil can be found that water droplets can quickly moisten the copper foil (Fig. 4c). The silicon slurry can be coated uniformly on carbon-coated copper foil (Fig. 4d). Due to the amphiphilic nature of the surface, where it is oily or water-based slurry, an electrode layer with good adhesion can be formed on the carbon-coated copper foil. The tensile testing results show that the tensile strength of carbon-coated copper foil (7.0 Kg_f) is better than that of bare copper foil (6.8 Kg_f) (Fig. 4e). In addition, when the carbon-coated copper foil with slurry was bent at 90° (Fig. 4f), the carbon-coated layer was not fall off and no powder falls. Then, to evaluate the adhesion strength of carbon-coated copper foil, it was measured by scratch testing (Fig. 4g and Movie S1 for the operation video) and tape peel testing (Fig. 4h and Movie S2 for the operation video). The results show that the carbon-coated layer was not fall off, indicating that the conductive layer is tightly attached to the copper foil, so no cracks and peeling were observed during the rolling process. In addition, the carbon-coated copper foil was treated with oven for anti-oxidation test. It can be observed that the appearance of carbon-coated copper foil isn't changed in a 200 °C oven after 30 min, indicating it has good anti-oxidation property (Fig. 4i), We also immerse the carbon-

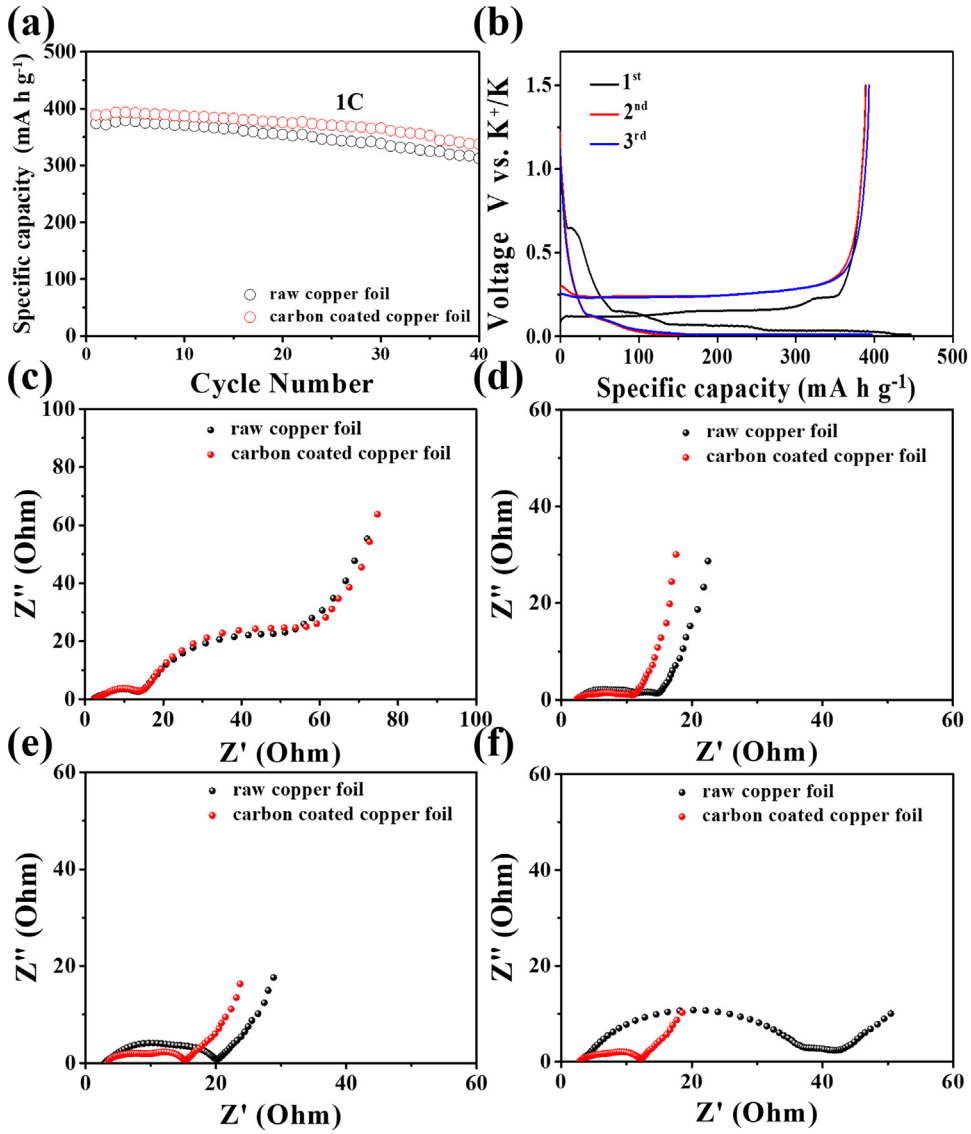

Fig. 6. Electrochemical performance of graphite half-cell made of bare copper foil and carbon-coated copper foil. Cycling performance of graphite half cells made of bare copper foil and carbon-coated copper foil at rates of (a) 1C and (b) 0.1C to 4C. Nyquist plots of graphite half cells made of bare copper foil and carbon-coated copper foil (c) before cycling, after (d) 20 cycles, (e) 40 cycles and (f) 120 cycles.

coated copper foil in polar (ethanol, isopropanol, NMP, and DI water) and non-polar (acetone, hexane, and toluene) solvents and treated with ultrasonic waves for 20 min (Fig. 4j). The carbon layer is not peeled off the copper foil in most solvent, only some peeling off in water (pink circle). In fact, the carbon-coated copper foil remains unchanged after being placed in various solvents for a month, indicating that the solvent resistance was good, and the adhesion of the conductive layer to the copper foil was well.

The bare copper foil and the carbon-coated copper foil were tested for the adhesion strength of electrode slurry through a universal testing machine. The adhesion of the carbon-coated copper foil increased from 0.409 Kg_f to 0.427 Kg_f, as shown in Fig. 5a and b. The tensile testing results show that the tensile strength of carbon-coated copper foil (7.0 Kg_f) is better than that of bare copper foil (6.8 Kg_f) (Fig. 5c). We use the four-point probe to measure resistance of the film to see whether the carbon-coated copper foil affects electrical properties due to the carbon layer. The electrical conductivity results show that there is little difference in electrical conductivity between carbon-coated copper foil and bare copper foil (Table 1). Figure S2 shows the cycle performance of carbon-coated copper foil directly assembled into a lithium-ion half-cell at 1C. The capacity can maintain about 70 mA h g^{-1} at 1C after 50 cycles and exhibits no recession so that the carbon-coated copper foil shows good cycling stability. Therefore, as the collector of the negative electrode on LIB, the performance of battery cannot be affected. Figure S3 shows the SEM images of the carbon-coated copper foil charged after 10 cycles (Figures S3a-c) and 100 cycles (Figures S3d-f) at 1C. The morphology of the two samples generally did not change significantly. The cross section images show that the SEI layer has been fully grown, and graphene can be clearly observed. In addition, it is also observed that most graphene maintains a uniform and large-scale structure after 100 cycles (Figure S3e and f).

The graphite anode slurry was coated on bare copper foil and carbon-coated copper foil, respectively, to form lithium-ion half-cells. As shown in Fig. 6a, the cycling stability of the two is similar after 40 cycles at 1C (1C = 372 mA h g^{-1}). The specific capacity of the bare copper foil and the carbon-coated copper foil are 312 and

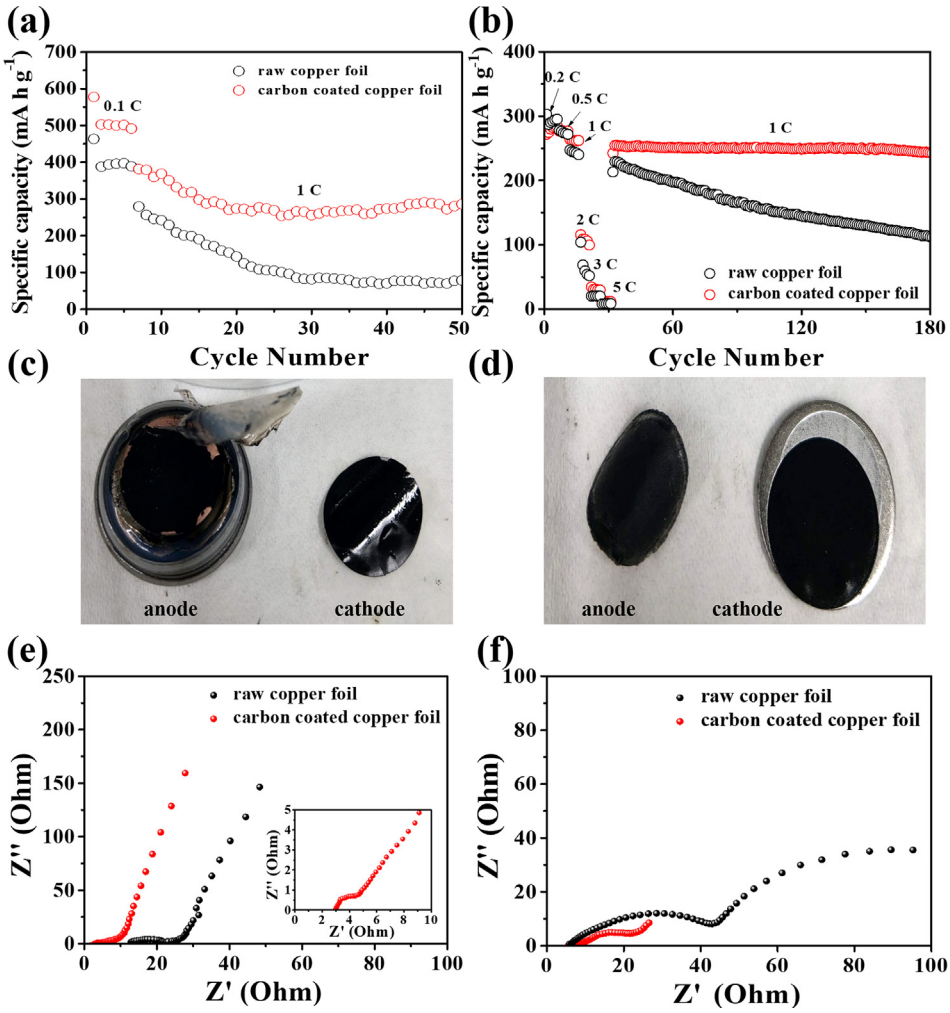

Fig. 7. Electrochemical performance of graphite coin-type full-cell made of bare copper foil and carbon-coated copper foil. (a) Cycling performance of graphite coin-type full cells made of bare copper foil and carbon-coated copper foil at rates of 1C. (b) Rate performance of graphite coin-type full cells made of bare copper foil and carbon-coated copper foil. The appearance of the electrode materials on (c) a bare copper foil and (d) a carbon-coated copper foil after 50 cycles. Nyquist plots of graphite coin-type full cells made of bare copper foil and carbon-coated copper foil (e) before cycling and (f) after cycles.

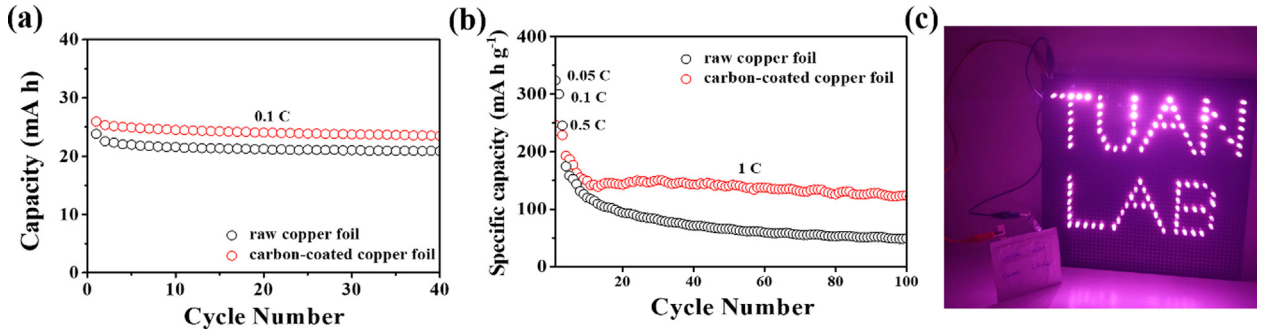

Fig. 8. Electrochemical performance of graphite pouch-type full cells made of bare copper foil and carbon-coated copper foil. Cycling performance of graphite pouch-type full cells made of bare copper foil and carbon-coated copper foil at rates of (a) 0.1C and (b) 1C. (c) A graphite pouch type full cells made of carbon-coated copper foil lighted up 100 LED bulbs.

337 mA h g^{-1}, respectively. Fig. 6b shows the performance at various current densities from 0.1C to 4C. Cells using carbon-coated copper foil can provide capacities of 536.9, 413.3, 320.8, 220.4, 167.6, and 115.2 mAh/g, whereas the bare copper foil provides the reversible capacity of 459.8, 309.1, 235.4, 173.1, 117.8 and 90.6 mAh/g at rates of 0.1, 1, 2, 2.5, 3 and 3.5C, respectively. When the rate returns from 4C to 0.1C, the capacities of bare copper foil and carbon-coated copper foil for graphite half-cells are 251.3 and

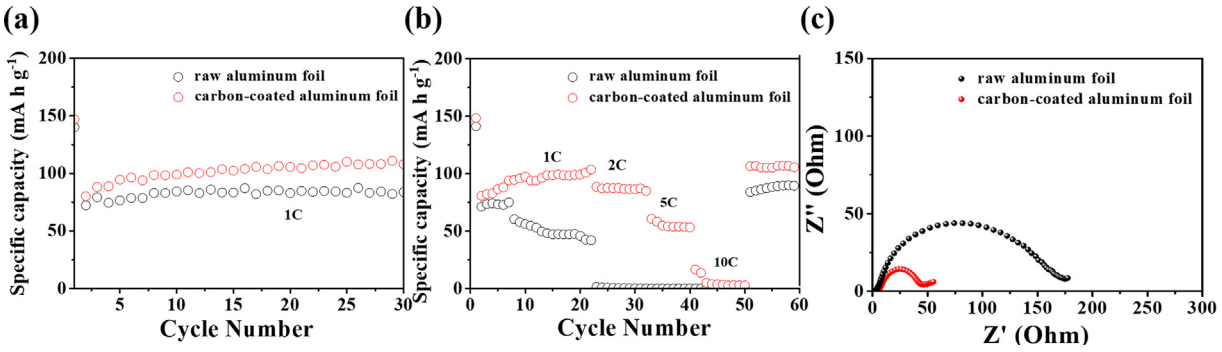

Fig. 9. Electrochemical performance of $LiFePO_4$ half-cell made of bare aluminum foil and carbon-coated aluminum foil. (a) Cycling performance of half cells made of bare aluminum foil and carbon-coated aluminum foil at rates of 1C. (b) Rate performance of half cells made of bare aluminum foil and carbon-coated aluminum foil. (c) Nyquist plots of half cells made of bare aluminum foil and carbon-coated aluminum foil after 60 cycles.

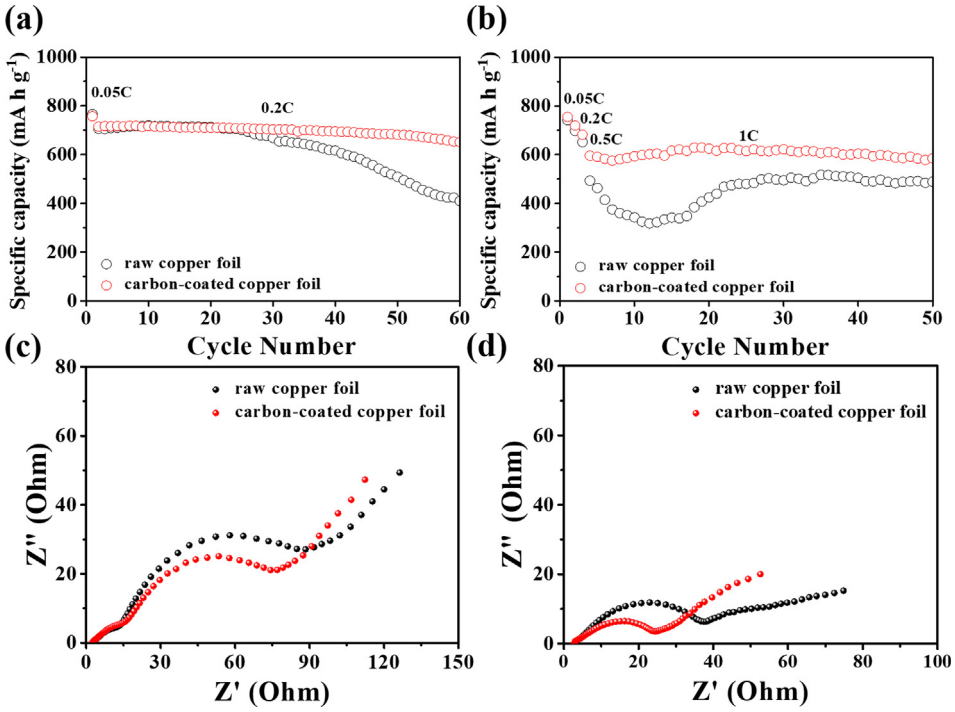

Fig. 10. Electrochemical performance of silicon-carbon anode with bare copper foil or carbon-coated copper foil as the current collector. Cycling performance of silicon-carbon full-cell made of bare copper foil and carbon-coated copper foil at rates of (a) 0.2C and (b) 1C. Nyquist plots of silicon-carbon half-cell made of bare copper foil and carbon-coated copper foil (c) before cycles and (d) after 10 cycles.

329.3 mAh/g, respectively. This result shows that the performance of carbon-coated copper foil is better than bare copper foil at high rates. It is found that the charge–discharge curve of the second cycle and the third cycle almost overlap, in addition to the capacity loss in the first cycle, indicating that a stable solid electrolyte interface (SEI) layer is generated in the first cycle. The impedance of the graphite half-cell was investigated by electrochemical impedance spectroscopy (EIS), shown in Fig. 6c-f. The impedance of the carbon-coated copper foil is similar to the bare copper foil before charge–discharge cycle (Fig. 6c), and after 20 cycles, it can be seen that the impedance of two kinds of the copper foil decrease (Fig. 6d). Among them, the impedance of the carbon-coated copper foil decreases obviously. After 40 cycles, the impedance of bare copper foil is greater than that of carbon coated copper foil (Fig. 6e). After 120 cycles, the impedance of the bare copper foil increases significantly, whereas the carbon-coated copper foil doesn't increase (Fig. 6f). More importantly, the impedance of half-cell prepared by carbon-coated copper foil is the smallest, which means that the conductive carbon-coated layer can effectively reduce the contact resistance during the cycle.

The graphite coin full-cell was investigated, as shown in Fig. 7a. After 50 cycles, the capacity of carbon-coated copper foil is higher the bare copper foil, 294 and 78 mA h g^{-1} at 1C, respectively, showing that the stability of carbon-coated copper foil is better. As displayed in Fig. 7b at different current densities, it was worth noting that the capacity can return to about 246 mA h g^{-1} when the current density regains 1C after 180 cycles, suggesting high stable cycle stability. However, the bare copper maintains merely the reversible capacity of 119 mA h g^{-1}. The capacities of carbon-coated copper foil and bare copper foil at various rates further demonstrate superb rate capability of the carbon-coated copper foil. Moreover, after the graphite coin-type full-cell was disassembled, as can be seen from Fig. 7c, the electrode material peels off from the bare copper foil after 50 cycles; in contrast, the electrode material is maintained well without peeling off on the carbon coated copper foil (Fig. 7d). Therefore, the carbon-coated layer

can increase the adhesion of the material on the copper foil and effectively prevent the material from peeling. Furthermore, the impedance of the graphite full-cell was investigated by EIS (Fig. 7e and f). Before charge–discharge cycle, the impedance of bare copper foil battery is larger than carbon-coated copper foil (Fig. 7e). Then, it can be observed that the impedance of the two increase after cycling (Fig. 7f), but it is found that the impedance of bare copper foil significantly increases. The reason why the impedance enhances is that the electrode materials are separated from the surface of the copper foil, consistent with the results of Fig. 7c.

The cycling stability of graphite pouch-type full-cell was investigated, as shown in Fig. 8a and b. The capacity of bare copper foil and carbon-coated copper foil at 0.1C after 40 cycles can be found that the trend is identical (Fig. 8a). In order to determine the difference between the two cells, the electrochemical performance of pouch-type full-cell was tested at 1C. After 100 cycles, the specific capacity of the bare copper foil and the carbon-coated copper foil are 49.15 and 123.88 mA h g^{-1}, respectively (Fig. 8b), suggesting the better stability of the carbon-coated copper foil. In addition, Fig. 8c shows that the pouch-type full-cell can power an TUAN LAB logo consisting of 100 red lightemitting diodes (LEDs) after the power is amplified more than 20 mA h.

The carbon-coated aluminum foil for $LiFePO_4$ half-cell was also studied. As shown in Fig. 9a, the specific capacity of the positive half-cell prepared with carbon-coated aluminum foil is 107 mA h g^{-1} at 1C for 30 cycles, and the specific capacity of the positive half-cell prepared with bare aluminum foil is 83 mA h g^{-1}. Additionally, it can be seen that the impedance of carbon-coated aluminum foil is effectively reduced, compared to the bare aluminum foil (Figure S5), corresponds to the results in the half-cell. Likewise, the rate performance of carbon-coated aluminum foil is further studied and compared with bare aluminum foil. As shown in Fig. 9b, the stability of carbon-coated aluminum foil is greater than bare aluminum foil at 1C. In addition, when the current density increases from 2C to 10C, the impedance of the bare aluminum foil is too large to withstand relatively high current densities, leading to unstable battery performance. Compared with the bare aluminum foil, the carbon-coated aluminum foil can still maintain 55 mA h g^{-1} at 5C. It means that the carbon-coated layer can indeed improve the conductivity of the material and the current collector. Fig. 9c shows that the carbon-coated aluminum foil can effectively reduce the impedance of the battery after charge–discharge cycle.

We also develop a silicon-carbon composite anode with silicon content of 20 wt% to investigate the effect of carbon-coated copper foil for silicon-carbon batteries. The 20 wt% silicon-carbon full-cell made by carbon-coated copper foil and bare copper foil was studied at 0.2C (Fig. 10a). After 60 cycles, the bare copper foil and carbon-coated copper foil maintained the specific capacity of 409.8 and 651.2 mA h g^{-1}, respectively, and the retention rate of carbon-coated copper foil (91%) is better than bare copper foil (59.4%). The results reveal that the silicon-carbon full-cell with carbon-coated copper foil has longer cycle-life. Then, increasing the current density can clearly distinguish the performance between the two cells. Fig. 10b shows that the carbon-coated copper foil and bare copper foil maintain the specific capacity of 585.3 and 489.3 mA h g^{-1} at 1C after 50 cycles, respectively. Importantly, the retention rate of carbon-coated copper foil is 92.2%, indicating that carbon-coated copper foil can effectively improve cycle stability of the silicon-carbon full-cell and increase capacity. As shown in EIS measurements (Fig. 10c and d), both the impedances of bare copper foil battery are larger than carbon-coated copper foil before and charge–discharge cycles. Fig. 11a and c show that the electrode materials peel off from the bare copper foil after 120 cycles, leading to a rapid decline in cycle life. In contrast, after 200 cycles, the electrode materials on carbon-coated copper foil can still be completely retained (Fig. 11b and d), indicating that the carbon-coated layer can increase the adhesion of the material on the copper foil and effectively avoid peeling off.

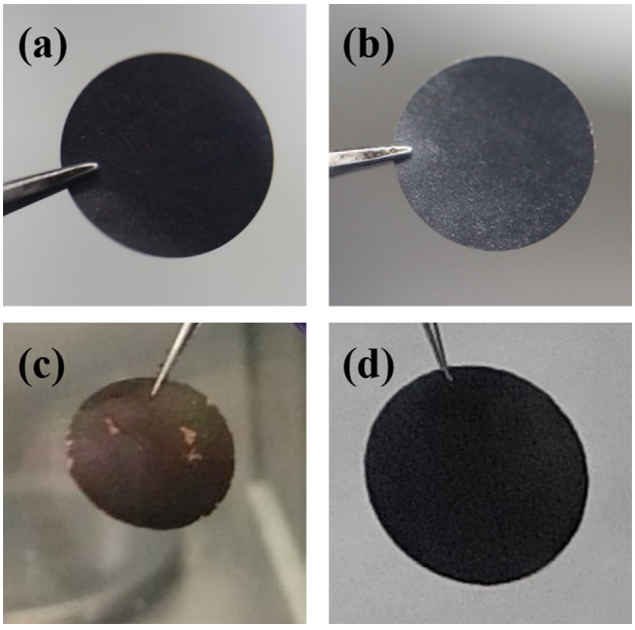

Fig. 11. Electrochemical test of silicon-carbon half cells made of bare copper foil and carbon-coated copper foil. The optical image of electrode materials of (a, c) bare copper foil and (b, d) carbon-coated copper foil on silicon-carbon half-cell after 120 and 200 cycles, respectively.

4. Conclusions

We develop an effective method to obtain carbon ink composed of disperse carbon materials, binders, and additives in a solvent via a wet ball milling method. The ink is coated on the surface of the metal sheet to obtain a conductive carbon coating layer with a thickness of about 1 μm. Compared with traditional copper foil, carbon-coated metal foil has good electrical conductivity, high specific surface area, oxidation resistance, and has better deformability than bare metal foil. The carbon coating can effectively reduce dynamic internal resistance of batteries, thereby reducing the interface resistance between the active material and the current collector. The active material has a strong interaction and adhesion force on the carbon layer, thereby improving the problem regarding large volume change of carbon or silicon-carbon anodes during cycling. This method is also compatible with the existing battery coating equipment and easy to operate, and has low cost for large-scale production realization, which can be used for the next-generation current collectors of LIBs or other energy storage devices.

CRediT authorship contribution statement

Kuan-Ting Chen: Conceptualization, Methodology, Data curation, Investigation. **Yi-Chun Yang:** Methodology, Data curation. **Yuan-Hsing Yi:** Data curation. **Xiang-Ting Zheng:** Data curation. **Hsing-Yu Tuan:** Supervision, Conceptualization, Writing - review & editing.

Declaration of Competing Interest

The authors declare that they have no known competing financial interests or personal relationships that could have appeared to influence the work reported in this paper.

Acknowledgements

We acknowledge the financial support by the Ministry of Science and Technology through the grants of MOST 108-2636-E-007-013, MOST 108-2622-8-007-016, MOST and MOST 109-2636-E-007-011 and by National Tsing Hua University through the grant of 107Q2708E1.

Appendix A. Supplementary data

Supplementary data to this article can be found online at https://doi.org/10.1016/j.jcis.2021.03.146.

References

[1] H. Xu, H. Jin, Z. Qi, Y. Guo, J. Wang, Y. Zhu, H. Ji, Graphene Foil as a Current Collector for NCM Material-Based Cathodes, Nanotechnology 31 (2020) 205710.
[2] S. Schweidler, L. de Biasi, A. Schiele, P. Hartmann, T. Brezesinski, J. Janek, Volume Changes of Graphite Anodes Revisited: A Combined Operando X-ray Diffraction and In Situ Pressure Analysis Study, J. Phys. Chem. C 122 (2018) 8829–8835.
[3] J. Heiska, M. Nisula, M. Karppinen, Organic Electrode Materials with Solid-State Battery Technology, J. Mater. Chem. A 7 (2019) 18735–18758.
[4] S.-H. Choi, G. Nam, S. Chae, D. Kim, N. Kim, W.S. Kim, J. Ma, J. Sung, S.M. Han, M. Ko, H.-W. Lee, J. Cho, Robust Pitch on Silicon Nanolayer-Embedded Graphite for Suppressing Undesirable Volume Expansion, Adv. Energy Mater. 9 (2019) 1803121.
[5] H.D. Chen, Z.L. Wang, X.H. Hou, L.J. Fu, S.F. Wang, X.Q. Hu, H.Q. Qin, Y.P. Wu, Q. Ru, X. Liu, S.J. Hu, Mass-Producible Method for Preparation of a Carbon-Coated Graphite@Plasma Nano-Silicon@Carbon Composite with Enhanced Performance as Lithium Ion Battery Anode, Electrochim. Acta 249 (2017) 113–121.
[6] D.J. Pereira, J.W. Weidner, T.R. Garrick, The Effect of Volume Change on The Accessible Capacities of Porous Silicon-Graphite Composite Anodes, J. Electrochem. Soc. 166 (2019) A1251–A1256.
[7] Y. Son, N. Kim, T. Lee, Y. Lee, J. Ma, S. Chae, J. Sung, H. Cha, Y. Yoo, J. Cho, Calendering-Compatible Macroporous Architecture for Silicon-Graphite Composite toward High-Energy Lithium-Ion Batteries, Adv. Mater. 37 (2020) 2003286.
[8] Q. Xu, J.K. Sun, Y.X. Yin, Y.G. Guo, Facile Synthesis of Blocky SiOx/C with Graphite-Like Structure for High-Performance Lithium-Ion Battery Anodes, Adv. Funct. Mater. 28 (2017) 1705235.
[9] M.M. Loghavi, M. Askari, M. Babaiee, A. Ghasemi, Improvement of the Cyclability of Li-ion Battery Cathode Using a Chemical-Modified Current Collector, J. Electroanal. Chem. 841 (2019) 107–110.
[10] W. Yuan, J. Luo, Z.G. Yan, Z.H. Tan, Y. Tang, High-Performance CuO/Cu Composite Current Collectors with Array-Pattern Porous Structures for Lithium-Ion Batteries, Electrochim. Acta 226 (2017) 89–97.
[11] X. Liu, D. Wang, B. Zhang, C. Luan, T. Qin, W. Zhang, D. Wang, X. Shi, T. Deng, W. Zheng, Vertical Graphene Nanowalls Coating of Copper Current Collector for Enhancing Rate Performance of Graphite Anode of Li Ion Battery: The Merit of Optimized Interface Architecture, Electrochim. Acta 268 (2018) 234–240.
[12] M.Z. Wang, H. Yang, K. Wang, S.L. Chen, H.N. Ci, L.R. Shi, J.Y. Shan, S.P. Xu, Q.C. Wu, C.Z. Wang, M. Tang, P. Gao, Z.F. Liu, H.L. Peng, Quantitative Analyses of the Interfacial Properties of Current Collectors at the Mesoscopic Level in Lithium Ion Batteries by Using Hierarchical Graphene, Nano Lett. 20 (2020) 2175–2187.
[13] C. Gao, N.D. Kim, R.V. Salvatierra, S.-K. Lee, L. Li, Y. Li, J. Sha, G.A.L. Silva, H. Fei, E. Xie, J.M. Tour, Germanium on Seamless Graphene Carbon Nanotube Hybrids for Lithium Ion Anodes, Carbon 123 (2017) 433–439.
[14] S. Bellani, E. Petroni, A.E. Del Rio Castillo, N. Curreli, B. Martín-García, R. Oropesa-Nuñez, M. Prato, F. Bonaccorso, Scalable Production of Graphene Inks via Wet-Jet Milling Exfoliation for Screen-Printed Micro-Supercapacitors, Adv. Funct. Mater. 29 (2019) 1807659.
[15] A.V. Tyurnina, I. Tzanakis, J. Morton, J. Mi, K. Porfyrakis, B.M. Maciejewska, N. Grobert, D.G. Eskin, Ultrasonic Exfoliation of Graphene in Water: A Key Parameter Study, Carbon 168 (2020) 737–747.
[16] G.T.T. Le, N. Chanlek, J. Manyam, P. Opaprakasit, N. Grisdanurak, P. Sreearunothai, Insight Into the Ultrasonication of Graphene Oxide with Strong Changes in Its Properties and Performance for Adsorption Applications, Chem. Eng. J. 373 (2019) 1212–1222.
[17] T. Leydecker, M. Eredia, F. Liscio, S. Milita, G. Melinte, O. Ersen, M. Sommer, A. Ciesielski, P. Samorì, Graphene Exfoliation in the Presence of Semiconducting Polymers for Improved Film Homogeneity and Electrical Performances, Carbon 130 (2018) 495–502.
[18] K.S. Aneja, S. Bohm, A.S. Khanna, H.M. Bohm, Graphene Based Anticorrosive Coatings for Cr (VI) Replacement, Nanoscale 7 (2015) 17879–17888.
[19] L. Dong, Z. Chen, X. Zhao, J. Ma, S. Lin, M. Li, Y. Bao, L. Chu, K. Leng, H. Lu, K.P. Loh, A Non-Dispersion Strategy for Large-Scale Production of Ultra-High Concentration Graphene Slurries in Water, Nat. Commun. 9 (2018) 76.
[20] G. Bepete, E. Anglaret, L. Ortolani, V. Morandi, K. Huang, A. Pénicaud, C. Drummond, Surfactant-Free Single-Layer Graphene in Water, Nat. Chem. 9 (2017) 347–352.
[21] J.H. Ding, H.R. Zhao, H.B. Yu, A Water-Based Green Approach to Large-Scale Production of Aqueous Compatible Graphene Nanoplatelets, Sci. Rep. 8 (2018) 5567–5574.
[22] M. Yi, Z. Shen, A Review on Mechanical Exfoliation for the Scalable Production of Graphene, J. Mater. Chem. A 3 (2015) 11700–11715.
[23] X. Li, J. Shen, C. Wu, K. Wu, Ball-Mill-Exfoliated Graphene: Tunable Electrochemistry and Phenol Sensing, Small 15 (2019) 1805567.
[24] C.F. Burmeister, A. Kwade, Process Engineering with Planetary Ball Mill, Chem. Soc. Rev. 42 (2013) 7660–7667.
[25] Y. Rosen, R. Marrach, V. Gutkin, S. Magdassi, Thin Copper Flakes for Conductive Inks Prepared by Decomposition of Copper Formate and Ultrafine Wet Milling, Adv. Mater. Technol. 4 (2019) 1800426.
[26] A. Amiri, M.N.M. Zubir, A.M. Dimiev, K.H. Teng, M. Shanbedi, S.N. Kazi, S.B. Rozali, Facile, Environmentally Friendly, Cost Effective and Scalable Production of Few-Layered Graphene, Chem. Eng. J. 326 (2017) 1105–1115.
[27] X. Fan, D.W. Chang, X. Chen, J. Baek, L. Dai, Functionalized Graphene Nanoplatelets from Ball Milling for Energy Applications, Curr. Opinion Chem. Eng. 11 (2016) 52–58.
[28] I.Y. Jeon, S. Zhang, L. Zhang, H.J. Choi, J.M. Seo, Z. Xia, L. Dai, J.B. Baek, Edge-Selectively Sulfurized Graphene Nanoplatelets as Efficient Metal-Free Electrocatalysts for Oxygen Reduction Reaction: The Electron Spin Effect, Adv. Mater. 25 (2013) 6138–6145.
[29] W. Bauer, D. Nötzel, Rheological Properties and Stability of NMP Based Cathode Slurries for Lithium Ion Batteries, Ceramics Int. 40 (2014) 4591–4598.
[30] W. Bauer, D. Nötzel, V. Wenzel, H. Nirschl, Influence of Dry Mixing and Distribution of Conductive Additives in Cathodes for Lithium Ion Batteries, J. Power Sources 288 (2015) 359–367.
[31] A. Kraytsberg, Y. Ein-Eli, Conveying Advanced Li-ion Battery Materials into Practice The Impact of Electrode Slurry Preparation Skills, Adv. Energy Mater. 6 (2016) 1600655.
[32] M.I. Kairi, S. Dayou, N.I. Kairi, S.A. Bakar, B. Vigolo, A.R. Mohamed, Toward High Production of Graphene Flakes – A Review on Recent Developments in Their Synthesis Methods and Scalability, Mater. Chem. A 6 (2018) 15010–15026.
[33] J.H. Heo, D.H. Shin, M.H. Jang, M.L. Lee, M.G. Kang, S.H. Im, Highly Flexible, High-Performance Perovskite Solar Cells with Adhesion Promoted $AuCl_3$-Doped Graphene Electrodes, J. Mater. Chem. A 5 (2017) 21146–21152.
[34] H. Su, T. Wu, D. Cui, X. Lin, X. Luo, Y. Wang, L. Han, The Application of Graphene Derivatives in Perovskite Solar Cells, Small Methods 4 (2020) 2000507.
[35] S. Pourhashem, M.R. Vaezi, A. Rashidi, M.R. Bagherzadeh, Distinctive Roles of Silane Coupling Agents on the Corrosion Inhibition Performance of Graphene Oxide in Epoxy Coatings, Prog. Org. Coat. 111 (2017) 47–56.
[36] N.R. Wilson, P.A. Pandey, R. Beanland, R.J. Young, I.A. Kinloch, L. Gong, Z. Liu, K. Suenaga, J.P. Rourke, S.J. York, J. Sloan, Graphene Oxide: Structural Analysis and Application as a Highly Transparent Support for Electron Microscopy, ACS Nano 3 (2009) 2547–2556.
[37] S.S. Li, K.H. Tu, C.C. Lin, C.W. Chen, M. Chhowalla, Solution-Processable Graphene Oxide as an Efficient Hole Transport Layer in Polymer Solar Cells, ACS Nano 4 (2010) 3169–3174.
[38] H. Lee, N. Son, H.Y. Jeong, T.G. Kim, G.S. Bang, J.Y. Kim, G.W. Shim, K.C. Goddeti, J.H. Kim, N. Kim, H.-J. Shin, W. Kim, S. Kim, S.-Y. Choi, J.Y. Park, Friction and Conductance Imaging of sp^2- and sp^3-Hybridized Subdomains on Single-Layer Graphene Oxide, Nanoscale 8 (2016) 4063–4069.